Available online at www.sciencedirect.com
ScienceDirect
Journal of Power Sources 175 (2008) 621–624
JOURNAL OF POWER SOURCES
www.elsevier.com/locate/jpowsour

Short communication

Structure and electrochemical behaviour of metastable $Mg_{50}Ti_{50}$ alloy prepared by ball milling

S. Rousselot, M.-P. Bichat, D. Guay, L. Roué *

INRS-Énergie, Matériaux et Télécommunications, 1650 Blvd. Lionel-Boulet, Varennes, Québec, Canada J3X 1S2

Received 14 August 2007; received in revised form 8 September 2007; accepted 10 September 2007
Available online 14 September 2007

Abstract

A 50–50 mixture of Mg and Ti was milled for different times, and the cycling discharge capacities of the resulting compounds were evaluated in KOH media. From Rietveld refinement analysis of the X-ray diffraction patterns, it is shown that a metastable hcp $Mg_{50}Ti_{50}$ compound is formed after 20 h of milling. This material has a very low-electrochemical hydriding activity. However, in the presence of 10 wt.% Pd (added before milling), it displays a maximum discharge capacity of *ca.* 400 mAh g^{-1} after three charge/discharge cycles. The irreversible structural evolution of the $Mg_{50}Ti_{50}$ alloy from a hcp phase to a fcc phase upon cycling is demonstrated.

Keywords: Mechanical alloying; Mg–Ti alloys; Metal hydride; Ni–MH batteries; Rietveld refinement

1. Introduction

Issues concerning climate change and air pollution are creating an increasing interest for low-emission vehicles such as hybrid electric vehicles (HEVs). The nickel–metal hydride (Ni–MH) battery is the dominant advanced battery technology for HEV applications due to its good overall performance, safety and environmental friendliness. However, initiatives must be taken to reduce the cost and to improve the performance of the Ni–MH battery system in order to favour an increase of the rate of consumer acceptance for the HEV. For that purpose, MH electrodes that are less expensive and that have higher energy-power densities than the usual $LaNi_5$-based materials used by the majority of the Ni–MH battery manufacturers have to be developed.

Recently, promising results have been obtained with metastable $Mg_yTi_{(1-y)}$ thin films prepared by electron beam deposition and magnetron co-sputtering deposition [1,2]. A reversible capacity as high as 1750 mAh g^{-1} was reached for $Mg_{0.8}Ti_{0.2}$. The improved discharge performance was attributed to the face-centered-cubic (fcc) structure of the hydride phase. However, these synthesis methods are expensive and not adapted to the preparation of such materials in large scale and in powdered form as required by the Ni–MH battery manufacturers. Therefore, it is important to put some effort into the efficient production of bulk Mg–Ti-based metal hydrides. This is a major challenge considering the absence of stable Mg–Ti compounds, as illustrated by the Mg–Ti phase diagram [3]. Moreover, conventional metallurgical methods are hardly applicable because the melting point of Ti (1943 K) significantly exceeds the boiling point of Mg (1363 K). In this context, mechanical alloying appears to be an appropriate synthesis method. This technique has demonstrated its high efficiency to form a large variety of both equilibrium and non-equilibrium materials at room temperature, starting from blended elemental or pre-alloyed powders [4,5]. Upon milling, repeated ball-to-powder collisions induce mechanical deformations, introduce strain into the powder and, as a result, the crystallites fracture into smaller pieces down to the nanometer range. Repeated cold welding and fracture events minimize the diffusion distance between each compound, allowing the formation of alloys. This leads to the formation of materials with unique chemical, physical and mechanical properties. It has been successfully applied to the synthesis of various materials such as magnetic, tribologic, superplastic, catalytic and hydrogen storage materials [4,5].

Few papers deal with the synthesis of Mg–Ti alloys by mechanical alloying [6–9]. For instance, Liang and Schulz [6] reported the extended dissolution of Ti in Mg up to a maximum of 12.5 at.% upon milling of a Mg–20 at.% Ti mixture. A solid

* Corresponding author. Tel.: +1 450 929 8185; fax: +1 450 929 8102.
E-mail address: roue@emt.inrs.ca (L. Roué).

0378-7753/$ – see front matter © 2007 Elsevier B.V. All rights reserved.
doi:10.1016/j.jpowsour.2007.09.022

solubility extension of 24 at.% Mg in Ti was also achieved by milling [7]. The hexagonal-close-packed (hcp) structure of Mg and Ti was maintained through the milling process. In comparison, the maximum equilibrium solid solubility of Ti in Mg and Mg in Ti is about 0.1 and 0.7 at.%, respectively [3]. Also, the formation of a metastable Ti–3 wt.% Mg solid solution with a face-centered-cubic (fcc) structure was reported after consolidation by hot isostatic pressing of a milled Ti–9 wt.% Mg mixture [9].

In the present work, it is shown that a metastable hcp $Mg_{50}Ti_{50}$ alloy can be produced in powder form by high-energy ball milling. Its electrochemical hydrogen storage capacity is determined. The structural evolution of the alloy from a hcp phase to a fcc phase upon hydrogen charge is also demonstrated.

2. Experimental

Pure Mg (99.9%, chips, Norsk Hydro), Ti (99.5%, −325 mesh, Alfa Aesar) and Pd (99.9%, −325 mesh, Alfa Aesar) were used as starting materials. Two samples were prepared: $Mg_{50}Ti_{50}$ and $Mg_{50}Ti_{50}$ + 10 wt.% Pd, the latter one corresponding to the $(Mg_{50}Ti_{50})_{94}Pd_6$ composition. The mixture of the desired composition was introduced into a cylindrical steel crucible with one 14 mm and two 11 mm diameter steel balls, corresponding to a ball-to-powder mass ratio of 10:1 for $Mg_{50}Ti_{50}$ and 9:1 when palladium is added. The container was sealed under argon atmosphere. The milling was performed using a vibratory type mill (Spex 8000M) for a time varying from 2.5 to 40 h. The milling yields (defined as the ratio of the powder masses after and before milling) were higher than 70%, indicating the absence of excessive cold welding between the powder particles and the milling tools. The energy dispersive X-ray (EDX) analysis of the milled powders displayed an iron content of less than 1 at.%, reflecting the limited erosion of the container and balls, even after 40 h of milling.

X-ray diffraction (XRD) was performed using a Bruker D8 diffractometer with Cu Kα radiation. Rietveld analysis [10,11] of the X-ray diffraction data was done using the GSAS software [12].

The electrochemical charge/discharge cycling tests were performed on an Arbin BT2000 battery tester at room temperature in a 6 M KOH solution using a three-electrode cell. The working electrode was a compacted mixture of 100 mg of active material and 800 mg of graphite plus 20 mg of carbon black. The counter electrode was a nickel wire and the reference electrode was an Hg/HgO electrode (XR440 from Radiometer Analytical). The working electrode was charged at $-200\,mA\,g^{-1}$ for 3 h and discharged at $20\,mA\,g^{-1}$ up to 0 V versus Hg/HgO. For the XRD analyses of cycled materials, the working electrode was made of 200 mg of active material mixed with 800 mg of graphite and 20 mg of carbon black.

3. Results and discussion

3.1. Structural analysis

Fig. 1A shows the X-ray diffraction patterns of $Mg_{50}Ti_{50}$ for different milling durations. After 2.5 h of milling, the XRD pattern of the material displays the characteristic peaks of both Ti and Mg phases. After 5 h of milling, the diffraction peaks of Mg(Ti) are slightly displaced toward the higher (lower) 2θ angle, indicating a slight modification of the lattice parameter of both compounds. In addition, both sets of peaks are broader and have a reduced intensity, indicating some refinement of the structure. After 10 h of milling, the diffraction peaks between $2\theta = 30°$ and $2\theta = 45°$ become indistinct as they seem to merge into one another. After 15–20 h of milling, there is no trace of the characteristic peaks of either Mg or Ti. Instead, a broad peak centered at $2\theta \sim 37.5°$ is observed, with less intense peaks at $2\theta \sim 51.7°$, 61.9°, 67.3° and 74.2°. The diffraction peaks are broad, indicating further refinement of the structure. No change is observed in the XRD pattern for longer milling period.

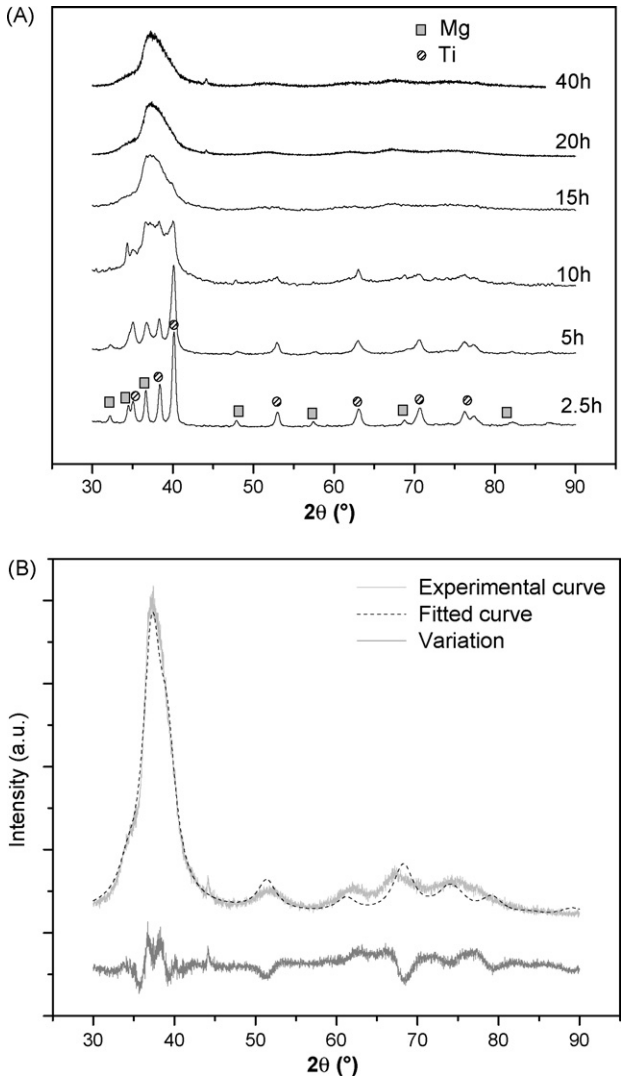

Fig. 1. (A) XRD patterns of $Mg_{50}Ti_{50}$ samples for different milling durations. (B) XRD pattern of 20 h milled $Mg_{50}Ti_{50}$ with Rietveld refinement data.

Rietveld refinement was performed to determine the structure of the compound formed after 20 h of milling, and the corresponding XRD data are presented in Fig. 1B, where plots of the experimental and calculated X-ray diffraction patterns are shown. The difference between the experimental data and the fitted curve is also shown at the bottom. The structure of Ti and Mg

was used as a starting point for Rietveld refinement. As shown in Fig. 1B, a reasonably good fit of the experimental XRD data could be obtained based on an hexagonal structure (space group *P*63/*mmc* (194), atomic position (1/3 2/3 1/4)), with $a = 3.03$ Å and $c = 4.84$ Å. These values are close to the average for the a and c lattice parameters of pure Mg ($a = 3.20$ Å and $c = 5.20$ Å) and pure Ti ($a = 2.91$ Å and $c = 4.68$ Å), suggesting that both Mg and Ti are dissolved (solid solution) in the hexagonal phase. As stated previously, the equilibrium solid solubility of Ti in Mg and Mg in Ti is about 0.1 and 0.7 at.%, respectively [3], well below the values suggested by the Rietveld refinement analysis of $Mg_{50}Ti_{50}$ milled for 20 h. High-energy ball milling has previously been shown to extend the solid solubility limits of the Mg–Ti system [6,7]. However, to the best of our knowledge, this is the first time that an extension of the solid solubility limit to the equimolar region of the Mg–Ti system is reported. After 20 h of milling, the crystallite size of the hcp phase is ~3 nm.

3.2. Electrochemical behaviour

The cycling discharge capacities of $Mg_{50}Ti_{50}$ milled for 20 h in the presence or not of 10 wt.% of Pd are presented in Fig. 2A. The $Mg_{50}Ti_{50}$ material milled without Pd displays a very low-electrochemical hydriding activity with a discharge capacity lower than 10 mAh g^{-1}. In the presence of palladium, the electrochemical activity is drastically improved. The initial discharge capacity is still low (about 20 mAh g^{-1}) but it increases greatly during the following cycles to reach, after only 3 charge/discharge cycles, a maximum discharge capacity of *ca.* 400 mAh g^{-1}. With further cycling, the discharge capacity decreases with a capacity decay rate of ~3% per cycle. It is noteworthy that the contribution of palladium to the whole discharge capacities is 18 mAh g^{-1} at most (considering a H/Pd atomic ratio of 0.7). In addition, on the basis of the XRD analysis (not shown), the structure of $Mg_{50}Ti_{50}$ is not modified by the addition of Pd. Further studies are in progress to understand precisely the key role played by Pd on the electrochemical activation of $Mg_{50}Ti_{50}$. In addition, work will have to be undertaken in order to replace palladium by a much less expensive catalyst since the requirement of 10 wt.% of Pd in the Mg–Ti-based alloys nullifies their economical advantage over the $LaNi_5$-based materials.

Fig. 2B presents the maximum discharge capacity (C_{max}) of $Mg_{50}Ti_{50}$–10 wt.% Pd compounds as a function of the milling time. In each case, C_{max} was attained after 3–4 charge/discharge cycles. As seen in Fig. 2B, C_{max} increases from 20 mAh g^{-1} after 2.5 h of milling, to about 400 mAh g^{-1} after 15 h of milling. Further increase of the milling duration does not improve the maximum discharge capacity. On the basis of the XRD patterns displayed in Fig. 1A, we can conclude that the increase of the C_{max} value is associated with the formation of the hcp $Mg_{50}Ti_{50}$ phase.

3.3. Structural evolution of the electrode material

The XRD pattern of the electrode made from as-milled 20 h $Mg_{50}Ti_{50}$–10 wt.% Pd is shown in the insert of Fig. 3. This XRD pattern is dominated by the diffraction peaks of graphite and carbon black added to improve the conductivity

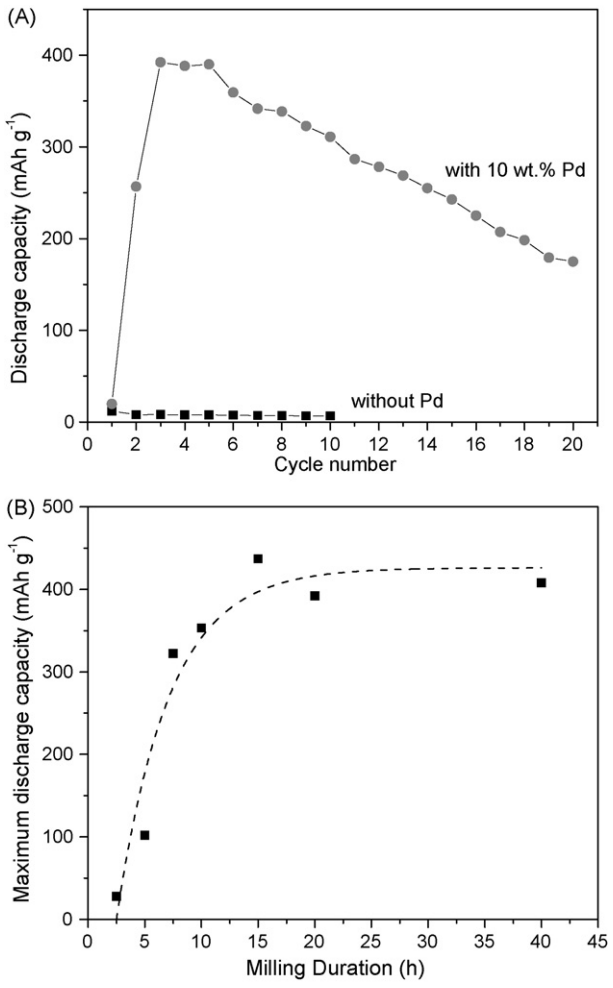

Fig. 2. (A) Cycling discharge capacities of $Mg_{50}Ti_{50}$ milled 20 h with and without 10 wt.% Pd. (B) Maximum discharge capacity for $Mg_{50}Ti_{50}$–10 wt.% Pd samples with varying milling duration.

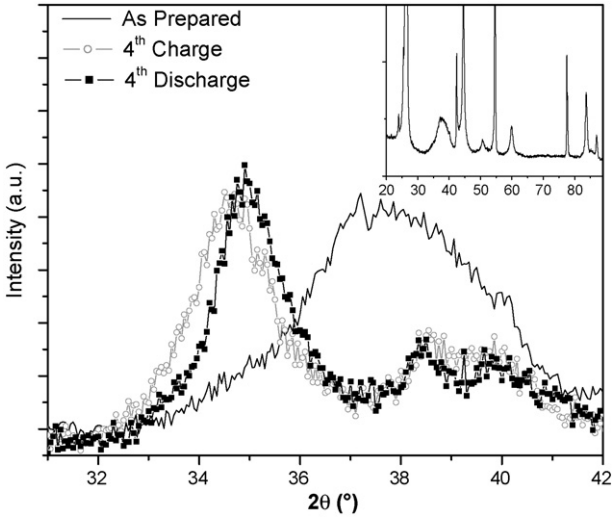

Fig. 3. XRD patterns of electrodes made from as-prepared $Mg_{50}Ti_{50}$–10 wt.% Pd milled during 20 h, and after the fourth charge and the fourth discharge cycle. The insert shows the whole XRD pattern of the as-prepared electrode.

of the electrode. However, a comparison of that curve with the XRD patterns of graphite and carbon black alone (not shown) reveals that only $Mg_{50}Ti_{50}$ contributes to the diffracted intensity in the region extending from $2\theta = 30^\circ$ to $2\theta = 42^\circ$. So, this region will be used to unravel the structural modification of the active electrode material as it goes through the successive charge/discharge cycles.

Fig. 3 shows the XRD pattern of 20 h milled $Mg_{50}Ti_{50}$–10 wt.% Pd after the fourth charge and the fourth discharge cycle. For the sake of comparison, the XRD pattern of as-prepared 20 h $Mg_{50}Ti_{50}$–10 wt.% Pd is also shown. Upon cycling, the intensity of the broad peak of the hcp phase centred at $2\theta \sim 37.8^\circ$ decreases. Instead, a new peak is observed at $2\theta \sim 34.7^\circ$ An XRD analysis conducted on an electrode made of pure 20 h $Mg_{50}Ti_{50}$–10 wt.% Pd (without the addition of graphite and carbon black) reveals that this peak forms simultaneously with four other peaks centered at ~38.8°, 58.3°, 70.1° and 73.4°. These peaks can be indexed to a fcc structure (space group $Fm\bar{3}m$) with $a = 4.4$ Å. Therefore, the C_{max} value of 20 h milled $Mg_{50}Ti_{50}$–10 wt.% Pd corresponds to a compound where the initially present hcp phase characteristic of milled $Mg_{50}Ti_{50}$ is transformed to a fcc phase. Such a hcp-to-fcc transition was also observed upon hydrogenation of Pd-containing Mg–Sc alloys [13] and by analogy, it was assumed that similar structural transition occurred with Pd-capped Mg–Ti thin films [1,2].

Upon discharge, the main diffraction peak of the charged material centered at $2\theta \sim 34.7^\circ$ does not disappear, indicating that the fcc structure does not revert back to the original hcp phase, and the formation of the fcc phase from the initial hcp phase appears to be irreversible. Instead, this peak is slightly displaced toward the larger 2θ angle values (from $2\theta \sim 34.7^\circ$ to $2\theta \sim 35.0^\circ$), indicating a slight decrease of the lattice parameter upon discharge.

A few other peaks are also observed in the XRD patterns of Fig. 3 at $2\theta = 38.5^\circ$ and 39.9°. The former peak is related to the formation of $Mg(OH)_2$, while the latter might be related to the presence of unalloyed nanocrystalline Pd. These issues will be sorted out in a forthcoming study.

4. Conclusion

The results reported in this paper demonstrate that a metastable hcp $Mg_{50}Ti_{50}$ alloy can be prepared by ball milling. Its electrochemical (de)hydrogenation requires the presence of Pd (10 wt.% added before milling). The compound reaches a maximum discharge capacity of 400 mAh g^{-1} after three charge/discharge cycles. The structure of the $Mg_{50}Ti_{50}$ alloy evolves from a hcp to a fcc structure upon cycling, and does not revert back to its original structure upon dehydrogenation.

Acknowledgements

This work has been financially supported by the Natural Sciences and Engineering Research Council of Canada (NSERC) and the "Fonds Québécois de la Recherche sur la Nature et les Technologies (FQRNT)".

References

[1] P. Vermeulen, R.A.H. Niessen, D.M. Borsa, B. Dam, R. Griessen, P.H.L. Notten, Electrochem. Solid State Lett. 9 (2006) A520.
[2] P. Vermeulen, R.A.H. Niessen, P.H.L. Notten, Electrochem. Commun. 8 (2006) 27.
[3] A.A. Nayeb-Hashemi, J.B. Clark, Phase diagrams of Binary Magnesium Alloys, ASM International, Metals Park, OH, 1998.
[4] L. Lü, M.O. Lai, Mechanical Alloying, Kluwer Academic Publishers, Norwell, USA, 1998.
[5] P.R. Soni, Mechanical Alloying Fundamentals and Application, Cambridge International Science Publishing, Cambridge, 2000.
[6] G. Liang, R. Schulz, J. Mater. Sci. 38 (2003) 1179.
[7] F. Sun, F.H. Froes, J. Alloys Compd. 340 (2002) 220.
[8] E. Zhou, C. Suryanarayana, F.H. Froes, Mater. Lett. 23 (1995) 27.
[9] C. Suryanarayana, F.H. Froes, J. Mater. Res. 5 (1990) 1880.
[10] H.M. Rietveld, Acta Crystallogr. 22 (1967) 151.
[11] H.M. Rietveld, J. Appl. Crystallogr. 2 (1969) 65.
[12] A.C. Larson, R.B. Von Dreele, General Structure Analysis System (GSAS), Los Alamos National Laboratory, Report LAUR 86-748, 2000.
[13] W.P. Kalisvaart, R.A.H. Niessen, P.H.L. Notten, J. Alloys Compd. 417 (2006) 280.